DOI: 10.1002/ejic.200701011

Theoretical Studies on $[Ru(bpy)_2(N^{\wedge}N)]^{2+}$ [N^N = Hydrazone and Azine]: Ground- and Excited-State Geometries, Electronic Structures, Absorptions, and Phosphorescence Mechanisms

Tao Liu,[a] Hong-Xing Zhang,*[a] Xin Zhou,[a] and Bao-Hui Xia[a,b]

Keywords: Ruthenium / Electronic structure / Spectroscopic properties / Density functional calculations

The ground- and excited-state geometries, electronic structures, absorptions, and emissions of two ruthenium(II) complexes $Ru(bpy)_2(N^{\wedge}N)$ [bpy = 2,2′-bipyridine, N^N = hydrazone (**1**) and azine (**2**)] were investigated theoretically. Their ground and the excited state geometries were fully optimized at the B3LYP/MP2/LANL2DZ and UB3LYP/UMP2/LANL2DZ levels, respectively, and the calculated geometries are consistent with the X-ray results. At the TD-DFT level with the PCM model, the absorptions and phosphorescence properties of **1** and **2** were calculated on the basis of the optimized ground- and excited-state geometries, respectively. The calculated lowest-lying absorptions of **1** (512 nm) and **2** (598 nm) are attributed to a $\{[d_{x^2-y^2}(Ru) + d_{xy}(Ru) + \pi(N^{\wedge}N)] \rightarrow [\pi^*(bpy)]\}$ transition with MLCT/LLCT transition characters and a $\{[d_{z^2}(Ru) + d_{xy}(Ru)] \rightarrow [\pi^*(N^{\wedge}N)]\}$ transition with dominant MLCT transition character, respectively. The calculated phosphorescence of **1** (638 nm) and **2** (731 nm) can be described as originating from a $^3\{[d_{x^2-y^2}(Ru) + d_{xy}(Ru) + \pi(N^{\wedge}N)] [\pi^*(bpy)]\}$ excited state with ^{3}MLCT/^{3}LLCT character and a $^3\{[d_{z^2}(Ru) + d_{x^2-y^2}(Ru)] [\pi^*(N^{\wedge}N)]\}$ excited state with dominantly ^{3}MLCT character, respectively. The calculated results showed that the modulation of the lowest ^{3}MLCT excited state of this kind of Ru complexes can be achieved by changing the N^N ligand from hydrazone to azine. Moreover, the fact that **2** displays phosphorescence but **1** does not can be interpreted by the different properties of the ^{3}MLCT excited state: the ^{3}MLCT excited state of **2** is more than 60 % occupied, whereas that of **1** is less than 20 % ($k_{r1} < k_{r2}$). The lowest-lying excited state of **1** is localized on the bpy ligand, whereas that of **2** lies on the N^N ligand, and the nonradiative decay pathways of **1** are easier than those of **2** ($k_{nr1} > k_{nr2}$).

Introduction

Recently, phosphorescent transition-metal complexes with d^6 electron configuration such as Ru^{II}, Rh^{III}, Os^{II}, and Ir^{III} have attracted considerable attention[1] due to their important roles as highly efficient electroluminescent (EL) emitters in the fields related to organic light emitting devices (OLEDs);[2] biological labeling reagents;[3] photocatalysts for CO_2 reduction;[4] and sensors for oxygen,[5] Ca^{2+},[6] Cu^{2+},[7] and Hg^{2+}[7] as well as for catalysts.[8] In theory, internal phosphorescence quantum efficiency can achieve as high as 100%, because the triplet metal-to-ligand charge transfer (^{3}MLCT) state can emit effectively by mixing the intensity of the ^{1}MLCT state by strong spin–orbital coupling effects of the transition metal.[9]

Furthermore, there has been continuous research activity towards Ru complexes. $Ru(bpy)_3^{2+}$ (bpy = 2,2′-bipyridine) is often taken as the model complex for tris(bidentate) ligands, as it has a triplet lowest-lying Ru(dπ) to bpy(π*) ^{3}MLCT excited state with a lifetime of ca. 1 μs.[10,11] Juris et al.[10] concluded that the photophysical properties of the chromophore are widely increased by modifying or changing any of the bipyridine ligands. Because of the strong MLCT transitions, high quantum yield, and the long-lived ^{3}MLCT excited state, Ru^{II} complexes have been applied in photoprocesses and OLEDs successfully.[12,13] Moreover, various Ru complexes have been extensively applied in other fields such as DNA,[14] dye-sensitized solar cells (DSSCs),[15] photocatalyst,[16] and so on.

It is necessary to create new transition-metal complexes to satisfy the needs in every field, but the design and synthetic procedures are difficult to realize. In fact, it is easier to synthesize emissive complexes by tuning the structure of the nonemissive transition-metal complexes skillfully. For example, Slugovc and coworkers[17] successfully synthesized a new series of cyclometalated iridium complexes $(ppy)_2Ir(Q)$ (Q = 8-quinolinolate, 5-formyl-8-quinolinolate, and 5-nitro-8-quinolinolate), and they found that $(ppy)_2Ir(Q)$ (Q = 8-quinolinolate) is not luminescent in aerated as well as in degassed solutions, but the complexes can emit in the orange to red region by adding formyl or nitryl groups at the 5-position of the 8-quinolinolate ligand. By investigating a series of Ru dihydrazone and substituted Ru dihydra-

[a] State Key Laboratory of Theoretical and Computational Chemistry, Institute of Theoretical Chemistry, Jilin University, Changchun 130023, People's Republic of China
E-mail: zhanghx@mail.jlu.edu.cn
[b] College of Chemistry, Jilin University, Changchun 130023, People's Republic of China

zone derivatives, Bolger et al.[18] concluded that Ru complexes with two hydrazone moieties are not emissive, but the $[Ru(bipy)_2(L–L)][PF_6]_2$ complexes with one hydrazone (bipy = 2,2′-bipyridine; L–L = 2-acetylpyridine phenylhydrazone, 2-acetylpyridine hydrazone) have good emissive properties. Moreover, Thompson and coworkers[19] investigated the absorption and emission spectra of $(ppy)_2Ir(acac)$ and $(ppy)_2Ir(dbm)$, and they found that $(ppy)_2Ir(acac)$ is a good candidate for OLEDs with a lifetime of 1.6 μs and a quantum efficiency of 0.34, but $(ppy)_2Ir(dbm)$ gives very weak phosphorescence with a quantum efficiency less than 0.01. The differences in the geometries should be responsible for the completely different quantum efficiencies. Moreover, on the basis of our previous theoretical studies,[20] different lowest-lying ^{3}MLCT excited states of $(ppy)_2Ir(acac)$ and $(ppy)_2Ir(dbm)$ should be responsible for the different phosphorescent abilities. Thus, the orbital nature of the lowest-lying excited state is obviously important for the spectroscopic properties of the transition-metal complexes; moreover, it is also an important factor for the luminescent ability of Ru^{II}-bipyridyl complexes.

Recently, Datta and coworkers[21] successfully synthesized two Ru complexes $[Ru(bpy)_2(N^\wedge N)]^{2+}$ [N^N = hydrazone (**1**) and azine (**2**)], and they also investigated the absorption and emission spectra of **1** and **2** in acetonitrile solution. They found that **1** is not emissive at room temperature or at 80 K, but **2** shows an appreciable emission at ambient temperature (729 nm, τ = 42 ns, $\phi = 2\times10^{-3}$) as well as at 80 K (690 nm, τ = 178 ns, $\phi = 7\times10^{-3}$) by changing N^N from hydrazone to azine. Through the investigation on the transient absorption, they concluded that the different lowest-lying ^{3}MLCT excited state properties should be responsible for the different phosphorescent abilities of **1** and **2**. However, there is no theoretical report to investigate the detailed properties of emission and the lowest-lying triplet excited state from an electronic structure point of view; in fact, quantum-chemical calculations can offer great possibilities in the elucidation of the structural and electronic properties of both the ground and excited states of transition-metal complexes

In this work, we aimed at providing an in-depth theoretical understanding of the geometries and spectroscopic properties of **1** and **2**. Herein, we employed ab initio and density functional theory (DFT) methods to study the electronic structure and spectroscopic properties of **1** and **2** in the ground and the excited states. Notably, the relationship between the spectral properties and the N^N ligand as well as the localization of the lowest-lying triplet excited state were explored.

Computational Details and Theory

In this work, the ground- and excited-state geometries of **1** and **2** were fully optimized by the DFT[22] method with Becke's three-parameter functional and the Lee–Yang–Parr functional[23] (B3LYP) and unrestricted B3LYP (UB3LYP) approaches. Furthermore, the geometries were also optimized by second-order Møller–Plesset perturbation[24] (MP2) and unrestricted MP2 (UMP2) methods so that they could be compared to the optimized geometries obtain by the DFT method. Spin contamination due to the admixture of excitations of higher multiplicity was rather small: the expectation values of the spin operator $<S^2>$ are below 2.01 for triplet states. The B3LYP and the MP2 calculated results revealed that the ^{1}A ground states of **1** and **2** have electronic configurations of $[(59b)^2(61a)^2]$ and $[(70b)^2(72a)^2]$, respectively. On the basis of the optimized ground- and excited-state geometries and the molecular orbital compositions, absorption and emission spectra in CH_3CN media were calculated by time-dependent DFT[25] (TDDFT) associated with the polarized continuum model (PCM).[26] This kind of theoretical approach and calculation level has been proven to be reliable for transition-metal complex systems in our previous work.[27]

In the calculations, the quasirelativistic pseudopotentials of the Ru atoms proposed by Hay and Wadt[28] with 16 valence electrons were employed, and LANL2DZ basis sets associated with the pseudopotential were adopted. The basis sets were described as Ru (8s6p4d)/[3s3p2d], C and N (10s5p)/[3s2p], and H (4s)/[2s]. Thus, 362 basis functions and 240 electrons for **1** and 432 basis functions and 284 electrons for **2** were included in the calculations. All of the calculations were accomplished by using the Gaussian 03 software package[29] on an Origin/3900 server.

The calculated complexes display C_2 symmetry in both the ground and excited states. As shown in Figure 1, the z/C_2 axis is oriented through the Ru atom and divides the N^N ligand into two identical parts; the y axis is oriented through the N2 and N5 atoms. Under the C_2 symmetry and the basis sets employed, the 362 orbitals of **1** are reduced to 182a and 180b irreducible orbitals. Likewise, the 432 orbitals of **2** are reduced to 217a and 215b irreducible orbitals. All these orbitals were included in the DFT and the MP2 calculations in order to have all of the possible electron correlations in the present computational level.

Results and Discussion

The Ground-State Geometries and the Frontier Molecular Orbital Properties

The main optimized-geometry structural parameters of **1** and **2** in the ground state together with the X-ray crystal diffraction data[21] are given in Table 1, and the optimized geometries are shown in Figure 1. Vibrational frequencies were calculated for the optimized geometries of **1** and **2** to verify that each of the geometries is a minimum (no minus frequency) on the potential energy surface.

The optimized bond lengths, bond angles, and dihedral angles of **1** and **2** in the ground state are in general agreement with the corresponding experimental values.[21] The DFT results showed that the calculated bond lengths of Ru–N1 (2.085 Å), Ru–N2 (2.099 Å), and Ru–N3 (2.107 Å)

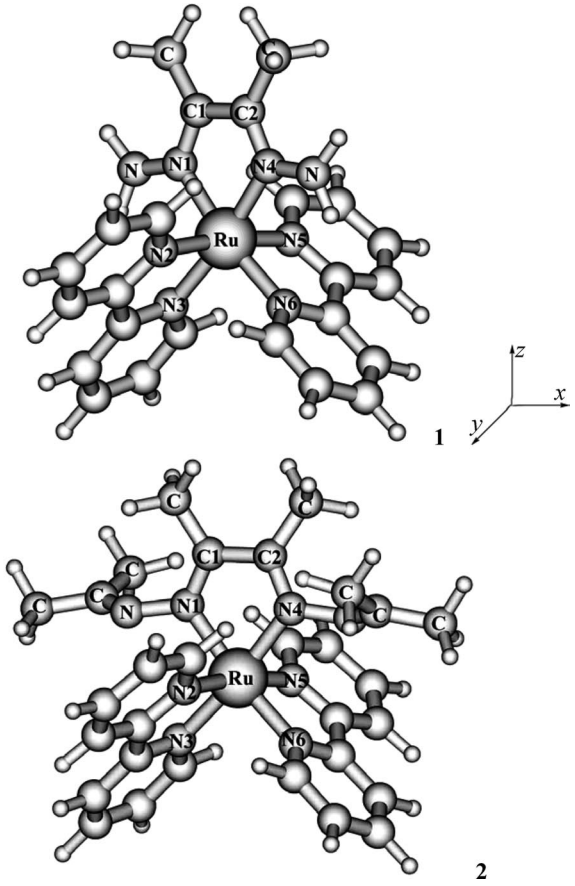

Figure 1. The optimized geometry structures of **1** and **2** at the B3LYP/LANL2DZ level.

of **1** are overestimated by 0.051, 0.039, and 0.029 Å, respectively, relative to the measured values. The bond lengths of **2** have similar trends to those of **1** in comparison with the measured values. The calculated bond angles N4–Ru–N1 (76.2°) and N2–Ru–N5 (172.8° for **1** and 172.2° for **2**) agree well with the measured values with a deviation less than 2°. The dihedral angles N1–C1–C2–N4 of **1** and **2** are 1.7° and 12.9°, respectively, which indicates that the N^N ligand of **1** is quasiplanar, but that of **2** has some distortion to break the planar structure because of the interactions of the large $=C(CH_3)_2$ substituent. The dihedral angles N2–Ru–N1–C1 of **1** and **2** are 96.4° and 99.5°, respectively, which indicates that the two bpy ligands and the N^N ligand are quasiperpendicular to each other. In comparison to the DFT results, the calculated results obtained by the MP2 method are more consistent with the measured results (with a deviation less than 0.02 Å for the bond length; see Table 1). The discrepancy between the calculated and the measured geometries is reasonable and acceptable, because the environments of the complexes are different: in the latter, the molecule is in a tight crystal lattice, whereas in the former the molecule is free.

The frontier molecular orbital compositions and energy levels of **1** and **2** are given in Tables 2 and 3, respectively. Table 2 shows that the LUMO (60b) and LUMO+1 (62a) of **1** are localized on the bpy ligand, whereas the LUMO+2 (61b) is localized on the N^N ligand. In compound **2**, the LUMO (71b) is dominantly localized on the N^N ligand, whereas the LUMO+1 (72b) and LUMO+2 (73a) have more than 90% π*(bpy). We can see that the change in the N^N ligand has a great effect on the composition of the low unoccupied molecular orbitals. With respect to the occupied molecular orbitals, Table 2 shows that the HOMO 61a of **1**, which lies at –5.91 eV, is dominantly composed of 19.5% $d_{x^2-y^2}$(Ru), 15.2% d_{xy}(Ru), and 57.4% π(N^N), whereas Table 3 shows that the HOMO 72a of **2** has 22.5% d_{z^2}(Ru), 42.5% d_{xy}(Ru), 15.7% π(N^N), and 13.3% π(bpy). Similarly, the MOs 59b of **1** and 70b of **2** are both composed of more than 70% Ru (d_{xz} and d_{yz}) and less than 30% ligand. HOMO-3 (59a) of **1** has 17.9% $d_{x^2-y^2}$(Ru), 26.8% d_{xy}(Ru), 13.3% π(bpy), and 41.4% π*(N^N), whereas the HOMO-3 (70a) of **2** is dominantly composed of the π(N^N) ligand with little d(Ru) composition. The four lower occupied molecular orbitals HOMO-4 (58b) and HOMO-5 (58a) of **1** as well as the HOMO-4 (69b) and HOMO-5 (69a) of **2**, with similar orbital energy levels of about –7.5 eV, are dominantly contributed by the bpy ligand. The energy levels and the component of the frontier molecular orbitals calculated by the MP2 method are similar to those calculated by the DFT method. On the basis of the above analysis, we found that the energy levels and the composition of the frontier molecular orbital can be significantly changed by tuning the N^N ligand from hydrazone to azine. Figure 2 shows the energy levels and the components of selected orbitals of **1** and **2**.

Table 1. Bond lengths [Å], bond angles [°], and dihedral angles [°] of **1** and **2** in the ground state and in the lowest-lying triplet excited state at the B3LYP/MP2 and UB3LYP/UMP2 levels, respectively, together with the experimental values.

	DFT				Exp.[a]		MP2			
	1		**2**		**1**	**2**	**1**		**2**	
State	A^1A	A^3B	A^1A	A^3B			A^1A	A^3B	A^1A	A^3B
Ru–N1	2.085	2.062	2.095	2.041	2.034	2.039	2.042	2.046	2.040	2.017
Ru–N2	2.099	2.100	2.103	2.102	2.060	2.053	2.075	2.080	2.076	2.087
Ru–N3	2.107	2.111	2.096	2.122	2.078	2.066	2.085	2.087	2.070	2.116
N4–Ru–N1	76.2	77.3	76.2	79.4	76.2	75.6	77.6	77.9	76.9	80.0
N2–Ru–N5	172.8	173.9	172.2	174.8	170.3	173.8	173.6	174.6	174.9	179.4
N1–C1–C2–N4	1.7	1.0	12.9	8.3	3.3	4.0	4.1	0.4	12.3	10.7
N2–Ru–N1–C1	96.4	96.1	99.5	97.7			96.8	96.6	101.7	96.6

[a] From ref.[21]

Table 2. Molecular orbital compositions [%] in the ground state for **1** at the B3LYP level.

Orbital	Energy [eV]	MO composition Ru	bpy	N^N	Main bond type	Ru component
61b L+2	–2.24	6.8	11.7	81.5	π*(N^N)	
62a L+1	–2.71	6.0	92.9	1.1	π*(bpy)	
60b L	–2.79	1.4	95.9	2.7	π*(bpy)	
HOMO–LUMO Energy Gap						
61a H	–5.91	35.1	7.5	57.4	$d_{x^2-y^2}+d_{xy}+\pi(N^\wedge N)$	19.5 $d_{x^2-y^2}$ 15.2 d_{xy}
60a H-1	–6.39	75.4	17	7.7	$d_{z^2}+d_{x^2-y^2}+\pi$(bpy)	53.9 d_{z^2} 13.0 $d_{x^2-y^2}$
59b H-2	–6.49	73.7	16.1	10.2	$d_{yz}+d_{xz}+\pi$(bpy)+π(N^N)	60.0 d_{yz} 13.3 d_{xz}
59a H-3	–6.68	45.3	13.3	41.4	$d_{x^2-y^2}+d_{xy}+\pi$(bpy)+π(N^N)	17.9 $d_{x^2-y^2}$ 26.8 d_{xy}
58b H-4	–7.55	0.6	99.1	0.3	π(bpy)	
58a H-5	–7.59	1.6	97.9	0.5	π(bpy)	

Table 3. Molecular orbital compositions [%] in the ground state for **2** at the B3LYP level.

Orbital	Energy [eV]	MO composition Ru	bpy	N^N	Main bond type	Ru component
73a L+2	–2.66	5.3	93.1	1.6	π*(bpy)	
72b L+1	–2.72	3.8	92.2	4.0	π*(bpy)	
71b L	–2.92	8.7	9.7	81.6	π*(N^N)	
HOMO–LUMO Energy Gap						
72a H	–6.14	71.0	13.3	15.7	$d_{z^2}+d_{xy}+\pi$(bpy)+π(N^N)	42.5 d_{xy} 22.5 d_{z^2}
71a H-1	–6.45	70.9	17.7	11.3	$d_{z^2}+d_{x^2-y^2}+\pi$(bpy)+π(N^N)	39.2 $d_{x^2-y^2}$ 29.5 d_{z^2}
70b H-2	–6.56	71.5	15.2	13.3	$d_{xz}+d_{yz}+\pi$(bpy)+π(N^N)	64.2 d_{xz} 7.0 d_{yz}
70a H-3	–7.28	11.3	6.0	82.7	$d_{x^2-y^2}+d_{xy}+\pi$(bpy)	5.2 $d_{x^2-y^2}$ 4.4 d_{xy}
69b H-4	–7.51	0.9	98.6	0.5	π(bpy)	
69a H-5	–7.55	1.6	97.1	1.3	π(bpy)	

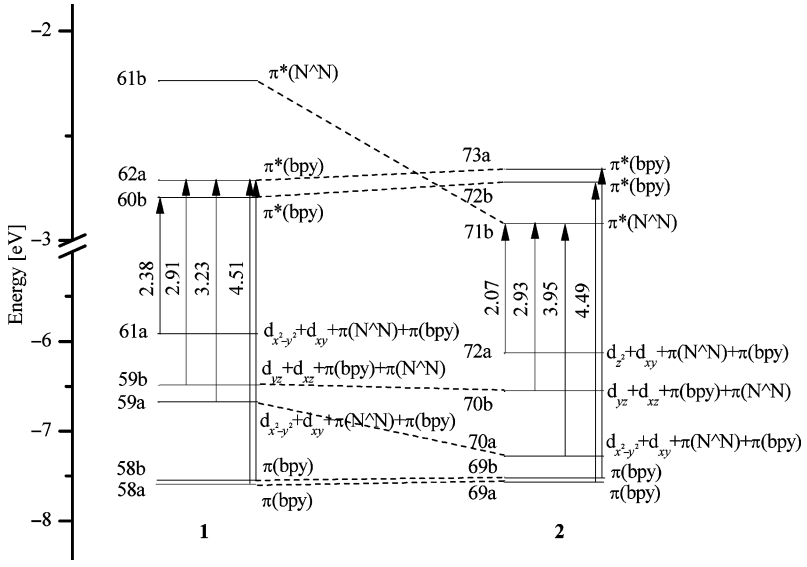

Figure 2. Diagrams of the molecular orbitals related to the absorptions of **1** and **2**.

Absorptions in CH_3CN Media

The calculated absorptions (singlet to singlet) and their oscillator strengths, the main configuration, their assignments, and the experiment values[21] are given in Table 4. Fitted Gaussian-type absorption curves with the calculated absorption data are shown in Figure 3. To intuitively understand the transition process, the energy levels and the properties of the molecular orbitals and the excitation energies involved in absorptions of **1** and **2** are displayed in Figure 2.

Table 4 shows that the lowest-lying absorptions of **1** and **2** are at 521 (2.38 eV) and 598 nm (2.07 eV), respectively. With respect to **1**, the absorption band at 521 nm is contributed by the excitation of MO 61a → MO 60b (|CI| = 0.685). Table 2 shows MO 61a is composed of 19.5% $d_{x^2-y^2}$(Ru), 15.2% d_{xy}(Ru), and 57.4% π(N^N), whereas MO 60b is dominantly localized on the bpy ligand; thus, the absorption at 521 nm can be dominantly assigned to a {[$d_{x^2-y^2}$(Ru) + d_{xy}(Ru) + π(N^N)] → [π*(bpy)]} transition with MLCT

Table 4. Calculated absorptions (TDDFT method) of **1** and **2** together with the experimental values.

	Transition	Config. (CI coeff.)	E/nm [eV]	Oscillator	Assignment	Expt.[a]/nm [eV]
1	$X^1A \rightarrow A^1B$	61a → 60b (0.685)	521 (2.38)	0.0111	MLCT/LLCT	
	$X^1A \rightarrow B^1B$	59b → 62a (0.615)	426 (2.91)	0.0607	MLCT/LLCT	420 (2.95)
	$X^1A \rightarrow C^1A$	59a→ 62a (0.631)	383 (3.23)	0.0435	MLCT/LLCT	
	$X^1A \rightarrow D^1B$	58b → 62a (0.380)	275 (4.51)	0.8472	ILCT	288 (4.31)
		58a → 60b (0.335)			ILCT	
2	$X^1A \rightarrow A^1B$	72a → 71b (0.655)	598 (2.07)	0.0003	MLCT/ILCT	
	$X^1A \rightarrow B^1A$	70b → 71b (0.591)	423 (2.93)	0.1633	MLCT/ILCT	440 (2.82)
	$X^1A \rightarrow C^1B$	70a → 71b (0.411)	314 (3.95)	0.2191	MLCT/ILCT	
	$X^1A \rightarrow D^1B$	69b → 73a (0.402)	276 (4.49)	0.7188	ILCT	288 (4.31)
		69a → 72b (0.364)			ILCT	

[a] From ref.[21]

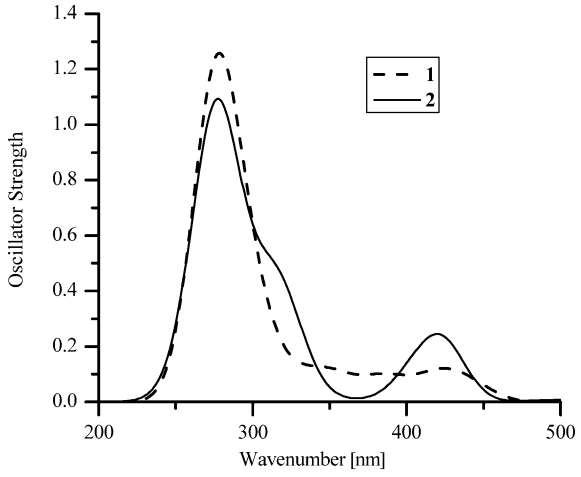

Figure 3. Simulated absorption spectra of **1** and **2** in CH_3CN media with the calculated data at the TD-B3LYP/LANL2DZ level.

and LLCT transition characters. For **2**, the excitation of MO 72a → MO 71b (|CI| = 0.655) is dominantly responsible for the absorption at 598 nm, and Table 3 shows that MO 72a has 42.5% d_{xy}(Ru), 22.5% d_{z^2}(Ru), 13.3% π(bpy), and 15.7% π(N^N), whereas MO 71b is contributed by π*(N^N). Thus, this absorption can be dominantly attributed to a {[d_{z^2}(Ru) + d_{xy}(Ru)] → [π*(N^N)]} transition with MLCT transition characters perturbed by a {[π*(N^N)] + [π*(bpy)] → [π*(N^N)]} transition with some ILCT/LLCT character. The absorption results showed that the transition properties of the lowest-lying absorption can be changed from MLCT/LLCT to MLCT/ILCT by tuning the N^N ligands from hydrazone to azine. The excitation energy level of the lowest-lying absorption based on the geometries optimized by the MP2 method is underestimated by ca. 0.01 and 0.05 eV for **1** and **2**, respectively.

Figure 3 shows that the distinguished absorption bands of **1** and **2** are at 426 and 423 nm, respectively. Table 4 shows that the excitation of MO 59b → MO 62a (|CI| = 0.615) contributes to the absorption of **1** at 426 nm. The results of the population analysis showed that MO 59b is dominantly contributed by 60.0% d_{yz}(Ru) and 13.3% d_{xz}(Ru) perturbed by some π(N^N and bpy), whereas MO 62a has a similar composition to MO 60b, which is dominantly contributed by π(bpy). Thus, this absorption can be described as a {[d_{yz}(Ru) + d_{xz}(Ru) + π(bpy)+ π(N^N)]} → [π*(bpy)] transition with dominantly MLCT and little ILCT/LLCT transition character (See Table 2). With respect to **2**, the distinguished absorption at 423 nm is contributed by excitation of MO 70b → MO 71b with the largest configuration coefficient of 0.591. Table 3 shows that MO 70b has 64.2% d_{xz}(Ru), 7.0% d_{yz}(Ru), 15.2% π(bpy), and 13.3% π(N^N), whereas MO 71b is dominantly localized on the N^N ligand. Thus, the absorption of **2** at 423 nm is attributed to a {[d_{xz}(Ru) + d_{yz}(Ru)] → [π*(N^N)]} transition with different MLCT transition characters from that of **1** at 426 nm.

Table 4 shows that the absorptions at 383 nm for **1** and 314 nm for **2** are contributed by excitations of MO 59a → MO 62a (CI = 0.631) and MO 70a → MO 71b (CI = 0.411), respectively. Upon discussion of the frontier molecular orbitals, the absorption of **1** at 383 nm can be ascribed to a {[$d_{x^2-y^2}$(Ru) + d_{xy}(Ru) + π(N^N)+π(bpy)] → [π*(bpy)]} transition with dominantly MLCT/LLCT transition character perturbed by little ILCT character, which is similar to the transition character of the lowest-lying absorption at 521 nm. With respect to **2**, Table 3 shows that MOs 70a and 71b are all dominantly contributed by the N^N ligand, so the absorption at 314 nm is dominantly assigned to a {[π(N^N)] → [π*(N^N)]} transition with ILCT transition character (Tables 2 and 3).

The absorptions of **1** and **2** at 275 and 276 nm, respectively, with the largest oscillator strength are contributed by two transitions. Table 4 shows that the excitations of MO 58b → MO 62a (|CI| = 0.380) and MO 58a → MO 62a (|CI| = 0.335) are responsible for the absorption of **1** at 275 nm, whereas the absorption of **2** at 276 nm is contributed by excitations of MO 69b → MO 73a (|CI| = 0.402) and MO 69a → MO 72b (|CI| = 0.364). Tables 2 and 3 show that MOs 58b, 58a, 62a of **1** and MOs 69b, 69a, 73a, 72b of **2** are dominantly localized on the bpy ligand. Thus, both of the absorptions can be described as a {[π(bpy)] → [π*(bpy)]} transition with ILCT transition character.

Upon experimentation,[21] the UV/Vis spectra of **1** and **2** in acetonitrile solution displayed a MLCT band in the 400 to 500 nm region, which is consistent with the calculated MLCT band at 400–500 nm in the excitation energy and the transition characters. The UV part of the absorption

was dominantly contributed by the π(bpy) → π*(bpy) transition around 288 nm for both **1** and **2** experimentally, which was confirmed by the calculated results that the absorption bands of **1** and **2** at 275 and 276 nm are assigned to the {[π(bpy)] → [π*(bpy)]} transition.

Triplet Excited-State Geometries and Emissions Spectra in CH_3CN

The main geometry structural parameters of **1** and **2** in A^3B excited states optimized by the UB3LYP and UMP2 methods are given in Table 1. The bond lengths, bond angles, and dihedral angles in the excited state are slightly distorted relative to those in the ground state, and two complexes show a similar variation trend. Moreover, the optimized geometries obtained by UB3LYP and UMP2 are consistent with each other. Herein, we take the UB3LYP results for example. The Ru–N1 bond lengths of **1** and **2** in the excited state are strengthened by 0.023 and 0.054 Å relative to those in the ground state, but the Ru–N3 bond lengths of **1** and **2** relax by about 0.004 and 0.026 Å, whereas the Ru–N2 bond lengths hardly changed, which indicates that the two bpy ligands have a trend to break away from the Ru atom, but the N^N ligand approaches the Ru center in the excited state. The excited-state bond angle N4–Ru–N1 of **1** and **2** increased by ca. 2–3° relative to those in the ground state, which indicates that the N4 and N1 atoms repel each other more intensely, and it is consistent with shortened Ru–N1 and Ru–N4 bond lengths. The excited-state bond angles N2–Ru–N5 of **1** and **2** increased by 1.1 and 2.6°, respectively, which indicates that the N2–Ru–N5 angle is more linear in the ground state. The N1–C1–C2–N4 dihedral angles of **1** and **2** are reduced by 0.7 and 4.7°, respectively, which indicates that the N^N ligand is more planar in the excited state than the ground state. The N2–Ru–N1–C1 dihedral angles of **1** and **2** are also reduced and approach 90° to make three ligands more perpendicular to each other in the excited state. The slight changes in the geometry result from the electron excitation from the d(Ru) to the π*(ligand) (vide infra). Interestingly, we found that the geometry changes in **2** are greater than those in **1** because the N^N ligand of **2** is larger than that of **1**, so the influence to the structures caused by excitation are greater in **2** than in **1**.

The calculated phosphorescence of **1** and **2** together with the measured value of **2**[21] are given in Table 5; the frontier molecular orbital compositions responsible for the emissions are summarized in Table 6. Figure 4 displays the intuitive electron transition diagram of the emission.

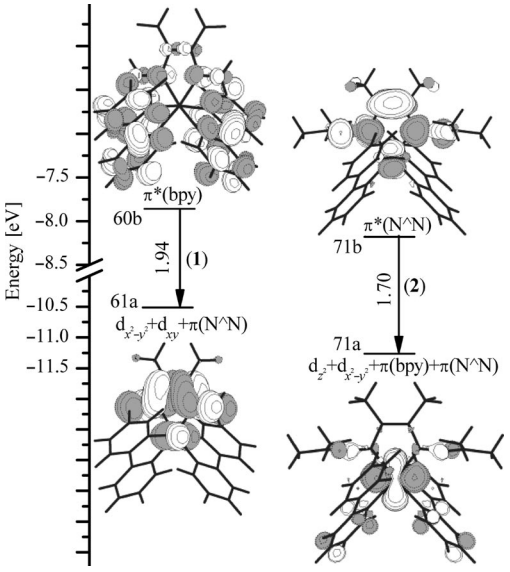

Figure 4. Transitions responsible for the calculated emission of **1** and **2** at 638 and 731 nm, respectively.

Table 5 shows that the calculated phosphorescence of **1** and **2** are at 638 (1.94 eV) and 731 nm (1.70 eV), respectively. The phosphorescence of **2** at 731 nm agrees very well with the experimental value at 729 nm (1.70 eV).[21] With respect to **1**, Table 5 shows that the transition of MO 60b → MO 61a with the configuration coefficient of 0.638 is responsible for the calculated emission at 638 nm. Table 6

Table 5. Calculated phosphorescent emissions (TDDFT method) of **1** and **2** together with the corresponding experimental values of **2**.

	Transition	Config. (CI coeff.)	E/nm [eV]	Assignment	Expt.[a]/nm [eV]
1	$A^3B \rightarrow X^1A$	60b → 61a (0.638)	638 (1.94)	^{3}MLCT/^{3}LLCT	
2	$A^3B \rightarrow X^1A$	71b → 71a (0.712)	731 (1.70)	^{3}MLCT/^{3}ILCT	729 (1.70)

[a] From ref.[21]

Table 6. Molecular orbital compositions [%] in the A^3B excited states for **1** and **2**.

Orbital	Energy	MO composition			Main bond type	Ru component
	[eV]	Ru	bpy	N^N		
1						
60b L	–7.86	0.4	87.0	12.6	π*(bpy)	
61a H	–10.50	20.0	4.2	75.8	$d_{x^2-y^2}+d_{xy}+\pi(N^\wedge N)$	12.7 $d_{x^2-y^2}$ 6.8 d_{xy}
2						
71b L	–8.16	13.9	7.8	78.3	π*(N^N)	
72a H	–10.65	52.1	8.8	39.1	$d_{xy}+d_{z^2}+\pi(N^\wedge N)$	36.6 d_{xy} 9.7 d_{z^2}
71a H-1	–11.27	73.5	16.4	10.1	$d_{z^2}+d_{x^2-y^2}+\pi(bpy)+\pi(N^\wedge N)$	42.8 d_{z^2} 30.4 $d_{x^2-y^2}$

shows that MO 60b is dominantly localized on the bpy ligand, whereas MO 61a is composed of 12.7% $d_{x^2-y^2}$(Ru), 6.8% d_{xy}(Ru), and 75.8% π(N^N). Thus, the calculated emission of **1** at 638 nm originates from the ^{3}\{[$d_{x^2-y^2}$(Ru) + d_{xy}(Ru) + π(N^N)] [π*(bpy)]\} excited state with ^{3}MLCT/^{3}LLCT character. However, the calculated emission of **2** at 731 nm has different transition character. The transition of MO 71b → MO 71a (|CI| = 0.712) contributes to the emission, and Table 6 shows that MO 71a has 42.8% d_{z^2}(Ru), 30.4% $d_{x^2-y^2}$(Ru), 16.4% π(bpy), and 10.1% π(N^N), whereas MO 71b is dominantly contributed by π*(N^N). Thus, the calculated emission of **2** at 731 nm can be dominantly described as originating from the ^{3}\{[d_{z^2}(Ru) + $d_{x^2-y^2}$(Ru)] [π*(N^N)]\} excited state with dominantly ^{3}MLCT character perturbed by little ^{3}\{[π(bpy) + π(N^N)] [π*(N^N)]\} excited state with ILCT/LLCT character, which is different from the lowest-lying triplet excited state of **1**.

The above discussion revealed that the lowest-lying absorptions calculated at 521 nm for **1** dominantly arise from the combination of MLCT and LLCT electronic transitions, and that those calculated at 598 nm for **2** arise from dominantly a MLCT transition, whereas their calculated phosphorescence are just the reverse processes of these lowest-lying absorptions because of the same symmetries and properties. The energy difference between the calculated lowest-energy absorption and the phosphorescence are 0.44 and 0.37 eV for **1** and **2**, respectively.

Upon experimentation, the following formulas exist: k_r (radiative decay rate), k_{nr} (nonradiative decay rate), Φ (quantum yield), and τ (lifetime), where $k_r = \Phi/\tau$, $k_{nr} = (1 - \Phi)/\tau$, and Φ can be affected by the competition between k_r and k_{nr}, namely, $\Phi = k_r/(k_r + k_{nr})$. So, in order to increase the quantum yield, k_r should be increased and k_{nr} should be decreased simultaneously or respectively.[1g,14c,30]

The calculated emission results showed that the excited state character of **1** and **2** are different from each other. The calculated emission of **1** originates from the ^{3}\{[d(Ru) + π(N^N)] [π*(bpy)]\} excited state with less than 20% ^{3}MLCT and more than 70% ^{3}LLCT. The emission of **2**, however, is dominantly from the ^{3}\{[d(Ru)] [π*(N^N)]\} excited state, with about 60% ^{3}MLCT and about 20% ^{3}ILCT/^{3}LLCT. In our previous study on the phosphorescence of Ir complexes,[20] we knew that the quantum efficiencies could be increased by larger ^{3}MLCT excited state compositions, which is consistent with the conclusion obtained by Abrahamsson et al.[21] that **1** is not emissive but **2** is at room temperature. On the investigation of Ru, Os, and Ir complexes, De Angelis et al.[1h,14c] and Chou, Chi et al.[31] concluded that intersystem crossing could be enhanced by notable ^{3}MLCT participation, namely, the phosphorescence ($T_1 \rightarrow S_0$ radiative transition) in which ^{3}ππ* mixed with ^{3}MLCT excited states should be greatly increased by increasing the ratio of ^{3}MLCT: ^{3}ππ*. This is consistent with our calculated results that the ^{3}MLCT composition of **2** is three times more than that of **1**. Thus, the increase in ^{3}MLCT should help the system to convey the excited-stated energy toward the emitting state and avoid higher-energy nonradiative decay pathways, ultimately leading to increased quantum yields, namely, $k_{r2} > k_{r1}$ and $\Phi_2 > \Phi_1$.

Complex **2** is emissive, but its quantum yield is only 2×10^{-3} and k_{nr2} (4.8×10^4 s^{-1}) is 500 times bigger than k_{r2} (2.4×10^7 s^{-1}).[21] This is a result of the fact that the effects of vibrational relaxation, quenching and energy transfer, internal conversion (IC), intersystem crossing (ISC), and interactions with the solvent molecules can prevent the system from undergoing radiative decay emission pathways, which ultimately leads to low quantum yields of **2**. Moreover, another reason why **2** is emissive but **1** is not is due to the fact that the interaction of **1** with the solvent is larger than that of **2**, because the hydrazone ligand is more planar, smaller, and more affected by the solvent than the azine ligand; thus, **1** can more easily convey the excited-state energy towards the nonradiative decay pathways than **2**, namely, $k_{nr1} > k_{nr2}$.

Furthermore, the ligand involved in the emission transition in the two complexes is different: for **1** the transition occurs on the bpy ligand, but for **2**, it occurs on the N^N ligand. Datta and coworkers deduced by transient absorption that the lowest ^{3}MLCT state of **2** is localized on the bpy ligand, which differs from our conclusion.[21] In order to confirm that our calculated result was more reasonable and acceptable, the emission spectra of **1** and **2** were recalculated by the TDDFT method on the basis of the excited-state geometry optimized at the UMP2/LANL2DZ level. Excited-state characters similar to those calculated by the DFT method were obtained, except for a small deviation in the excitation energy of about 0.09 eV for **1** and 0.14 eV for **2**. Both the ab initio and the DFT methods gave acceptable results, but the DFT results are more consistent with the experimental values.

Conclusions

The present theoretical work investigated the ground- and excited-state geometries, absorptions, and phosphorescence properties of two Ru complexes with bpy and N^N ligands. The calculated results showed that HOMO and LUMO can be significantly changed by altering the N^N ligand. The lowest-lying absorption of **1** at 521 nm was assigned to the MLCT/LLCT transition and that of **2** at 598 nm was dominantly ascribed to MLCT transitions. The calculated phosphorescence of **1** at 638 nm can be described as originating from the ^{3}MLCT/^{3}LLCT excited state, whereas that of **2** at 731 nm was dominantly from the ^{3}MLCT excited state. Compound **1** was found to be nonemissive, but the calculated results showed three reasons for the emission of **2**: (1) The different triplet lowest-lying excited state for **1** (^{3}MLCT/^{3}LLCT) and **2** (^{3}MLCT/^{3}ILCT). (2) The ^{3}MLCT excited state composition of **2** is three times more than that of **1** ($k_{r1} < k_{r2}$). (3) The nonradiative decay pathways are easier for **1** than for **2** ($k_{nr1} > k_{nr2}$). Thus, it is very practical to explore the factors related to k_r and k_{nr}, including the relationship between the N^N ligand, the ^{3}MLCT composition and the phosphorescence properties,

and the interactions between the Ru^{II} complexes and the solvent. We hope these theoretical studies can provide suggestions in the design of new highly efficient Ru^{II} phosphorescent materials.

Acknowledgments

This work was supported by the Natural Science Foundation of China (Grant Nos. 20173021, 20333050, and 20573042).

[1] a) V. Balzani, A. Juris, M. Venturi, S. Campagna, S. Serroni, *Chem. Rev.* **1996**, *96*, 759–834; b) A. Vlček Jr, *Coord. Chem. Rev.* **1998**, *177*, 219–256; c) K. D. Demadis, C. M. Hartshorn, T. Meyer, *J. Chem. Rev.* **2001**, *101*, 2655–2686; d) M. Lepeltier, T. K.-M. Lee, K. K. W. Lo, L. Toupet, H. L. Bozec, V. Guerchais, *Eur. J. Inorg. Chem.* **2007**, 2734–2747; e) B. Carlson, G. D. Phelan, W. Kaminsky, L. Dalton, X. Jiang, S. Liu, A. K. Y. Jen, *J. Am. Chem. Soc.* **2002**, *124*, 14162–14172; f) D. Amarante, C. Cherian, A. Catapano, R. Adams, M. H. Wang, E. G. Megehee, *Inorg. Chem.* **2005**, *44*, 8804–8809; g) Y. L. Tung, L. S. Chen, Y. Chi, P. T. Chou, Y. M. Cheng, E. Y. Li, G. H. Lee, C. F. Shu, F. I. Wu, A. J. Carty, *Adv. Funct. Mater.* **2006**, *16*, 1615–1626; h) F. De Angelis, S. Fantacci, N. Evans, C. Klein, S. M. Zakeeruddin, J.-E. Moser, K. Kalyanasundaram, H. J. Bolink, M. Grätzel, M. K. Nazeeruddin, *Inorg. Chem.* **2007**, *46*, 5989–6001.

[2] a) Y. Wand, N. Herron, V. V. Grushin, D. D. LeCloux, V. A. Petrov, *Appl. Phys. Lett.* **2001**, *79*, 449–451; b) H. Xin, F. Y. Li, M. Shi, Z. Q. Bian, H. Ch. Huang, *J. Am. Chem. Soc.* **2003**, *125*, 7166–7167; c) A. Tsuboyama, H. Iwawaki, M. Furugori, T. Mukaide, J. Kamatani, S. Igawa, T. Moriyama, S. Miura, T. Takiguchi, S. Okada, M. Hoshino, K. Ueno, *J. Am. Chem. Soc.* **2003**, *125*, 12971–12979; d) T. Tsuzuki, S. Tokito, *Adv. Mater.* **2007**, *19*, 276–280; e) P. T. Chou, Y. Chi, *Eur. J. Inorg. Chem.* **2006**, 3319–3332.

[3] a) K. K. W. Lo, C. K. Chung, T. K. M. Lee, L. H. Lui, K. H. K. Tsang, N. Y. Zhu, *Inorg. Chem.* **2003**, *42*, 6886–6897; b) K. K. W. Lo, D. C. M. Ng, C. K. Chung, *Organometallics* **2001**, *20*, 4999–5001.

[4] a) N. D. Silaware, A. S. Goldman, R. Ritter, D. R. Tyler, *Inorg. Chem.* **1989**, *28*, 1231–1236; b) K. A. Belmore, R. A. Vanderpool, J. C. Tsai, M. A. Khan, K. M. Nicholas, *J. Am. Chem. Soc.* **1988**, *110*, 2004–2005.

[5] a) R. Gao, D. G. Ho, B. Hernandez, M. Selke, S. A. Vinogradov, *J. Am. Chem. Soc.* **2002**, *124*, 14828–14829; b) M. C. DeRosa, D. J. Hodgson, G. D. Enright, B. Dawson, C. E. B. Evans, R. J. Crutchley, *J. Am. Chem. Soc.* **2004**, *126*, 7619–7626; c) G. Di Marco, M. Lanza, A. Mamo, I. Stefio, C. Di Pietro, G. Romeo, S. Campagna, *Anal. Chem.* **1998**, *70*, 5019–5023.

[6] M. L. Ho, F. M. Hwang, P. N. Chen, Y. H. Hu, Y. M. Cheng, K. S. Chen, G. H. Lee, Y. Chi, P. T. Chou, *Org. Biomol. Chem.* **2006**, *4*, 98–103.

[7] a) X. H. Li, Z. Q. Liu, F. Y. Li, X. F. Duan, C. H. Huang, *Chin. J. Chem.* **2007**, *25*, 186–189; b) M. A. Nolan, S. P. Kounaves, *Anal. Chem.* **1999**, *71*, 3567–3573; c) Q. Zhao, T. Y. Cao, F. Y. Li, X. H. Li, H. Jing, T. Yi, C. H. Huang, *Organometallics* **2007**, *26*, 2077–2081.

[8] a) A. Haynes, P. M. Maitlis, G. E. Morris, G. J. Sunley, H. Adams, P. W. Badger, C. M. Bowers, D. B. Cook, P. I. P. Elliott, T. Ghaffar, H. Green, T. R. Griffin, M. Payne, J. M. Pearson, M. J. Taylor, P. W. Vickers, R. J. Watt, *J. Am. Chem. Soc.* **2004**, *126*, 2847–2861; b) J. Oxgaard, G. Bhalla, R. A. Periana, W. A. Goddard III, *Organometallics* **2006**, *25*, 1618–1625.

[9] a) C. Adachi, M. A. Baldo, S. R. Forrest, M. E. Thompson, *Appl. Phys. Lett.* **2000**, *77*, 904–906; b) A. Harriman, J. Izzet, *Phys. Chem. Chem. Phys.* **2007**, *9*, 944–948.

[10] A. Juris, V. Balzani, F. Barigletti, S. Campagna, P. Belser, A. Von Zelewsky, *Coord. Chem. Rev.* **1988**, *84*, 85–277.

[11] M. K. DeArmond, M. L. Myrick, *Acc. Chem. Res.* **1989**, *22*, 364–370.

[12] a) J. P. Paris, W. W. Brandt, *J. Am. Chem. Soc.* **1959**, *81*, 5001–5002; b) P. G. Bradley, N. Kress, B. A. Hornberger, R. F. Dallinger, W. H. Woodruff, *J. Am. Chem. Soc.* **1981**, *103*, 7441–7446; c) H. Yersin, D. Braun, *Coord. Chem. Rev.* **1991**, *111*, 39–46.

[13] a) E. S. Handy, A. J. Pal, M. F. Rubner, *J. Am. Chem. Soc.* **1999**, *121*, 3525–3528; b) F. G. Gao, A. J. Bard, *J. Am. Chem. Soc.* **2000**, *122*, 7426–7427; c) H. Rudmann, S. Shimada, M. F. Rubner, *J. Am. Chem. Soc.* **2002**, *124*, 4918–4921; d) S. Fantacci, F. De Angelis, A. Selloni, *J. Am. Chem. Soc.* **2003**, *125*, 4381–4387.

[14] a) J. K. Barton, *Science* **1986**, *233*, 727–734; b) K. E. Erkkila, D. T. Odom, J. K. Barton, *Chem. Rev.* **1999**, *99*, 2777–2796; c) S. Fantacci, F. De Angelis, A. Sgamellotti, A. Marrone, N. Re, *J. Am. Chem. Soc.* **2005**, *127*, 14144–14145.

[15] a) H. E. Toma, K. Araki, *Coord. Chem. Rev.* **2000**, *196*, 307–329; b) Y. Ohsaki, N. Masaki, T. Kitamura, Y. Wada, T. Okamoto, T. Sekino, K. Niihara, S. Yanagida, *Phys. Chem. Chem. Phys.* **2005**, *7*, 4157–4163; c) M. K. Nazeeruddin, A. Kay, I. Rodicio, R. Humphry-Baker, E. Muller, P. Liska, N. Vlachopoulos, M. Grätzel, *J. Am. Chem. Soc.* **1993**, *115*, 6382–6390; d) J. E. Kroeze, N. Hirata, S. Koops, M. K. Nazeeruddin, L. Schmidt-Mende, M. Grätzel, J. R. Durrant, *J. Am. Chem. Soc.* **2006**, *128*, 16376–16383; e) M. K. Nazeeruddin, F. De Angelis, S. Fantacci, A. Selloni, G. Viscardi, P. Liska, S. Ito, B. Takeru, M. Grätzel, *J. Am. Chem. Soc.* **2005**, *127*, 16835–168471.

[16] a) S. Kadar, T. Amemiya, K. Showalter, *J. Phys. Chem. A* **1997**, *101*, 8200–8206; b) Y. Motoyama, K. Mitsui, T. Ishida, H. Nagashima, *J. Am. Chem. Soc.* **2005**, *127*, 13150–13151.

[17] S. Kappaun, S. Sax, S. Eder, K. C. Moller, K. Waich, F. Niedermair, R. Saf, K. Mereiter, J. Jacob, K. Mullen, E. J. W. List, C. Slugovc, *Chem. Mater.* **2007**, *19*, 1209–1211.

[18] J. A. Bolger, G. Ferguson, J. P. James, C. Long, P. McArdle, J. G. Vos, *J. Chem. Soc., Dalton Trans.* **1993**, 1577–1583.

[19] S. Lamansky, P. Djurovich, D. Murphy, F. Abdel-Razzaq, H. E. Lee, C. Adachi, P. E. Burrows, S. R. Forrest, M. E. Thompson, *J. Am. Chem. Soc.* **2001**, *123*, 4304–4312.

[20] T. Liu, B. H. Xia, X. Zhou, H. X. Zhang, Q. J. Pan, J. S. Gao, *Organometallics* **2007**, *26*, 143–149.

[21] M. Abrahamsson, L. Hammarström, D. A. Tochere, S. Nag, D. Datta, *Inorg. Chem.* **2006**, *45*, 9580–9586.

[22] E. Runge, E. K. U. Gross, *Phys. Rev. Lett.* **1984**, *52*, 997–1000.

[23] A. D. Becke, *J. Chem. Phys.* **1993**, *98*, 5648–5652.

[24] a) M. J. Frisch, M. Head-Gordon, J. A. Pople, *Chem. Phys. Lett.* **1990**, *166*, 275–280; b) M. J. Frisch, M. Head-Gordon, J. A. Pople, *Chem. Phys. Lett.* **1990**, *166*, 281–289; c) M. Head-Gorden, J. A. Pople, M. J. Frisch, *Chem. Phys. Lett.* **1988**, *153*, 503–506; d) M. Head-Gorden, T. Head-Gorden, *Chem. Phys. Lett.* **1994**, *220*, 122–128.

[25] a) R. E. Stratmann, G. E. Scuseria, *J. Chem. Phys.* **1998**, *109*, 8218–8224; b) N. N. Matsuzawa, A. Ishitani, *J. Phys. Chem. A* **2001**, *105*, 4953–4962; c) M. E. Casida, C. Jamorski, K. C. Casida, D. R. Salahub, *J. Chem. Phys.* **1998**, *108*, 4439–4449.

[26] a) M. Cossi, G. Scalmani, N. Regar, V. Barone, *J. Chem. Phys.* **2002**, *117*, 43–54; b) V. Barone, M. Cossi, *J. Chem. Phys.* **1997**, *107*, 3210–3221.

[27] a) T. Liu, H. X. Zhang, B. H. Xia, *J. Phys. Chem. A* **2007**, *111*, 8724–8730; b) X. Zhou, H. X. Zhang, Q. J. Pan, M. X. Li, Y. Wang, C. M. Che, *Eur. J. Inorg. Chem.* **2007**, 2181–2188; c) M. X. Li, H. X. Zhang, X. Zhou, Q. J. Pan, H. G. Fu, C. C. Sun, *Eur. J. Inorg. Chem.* **2007**, 2171–2180.

[28] a) P. J. Hay, W. R. Wadt, *J. Chem. Phys.* **1985**, *82*, 299–310; b) P. J. Hay, W. R. Wadt, *J. Chem. Phys.* **1985**, *82*, 270–283.

[29] M. J. Frisch, G. W. Trucks, H. B. Schlegel, G. E. Scuseria, M. A. Robb, J. R. Cheeseman, J. A. Montgomery Jr, T. Vreven, K. N. Kudin, J. C. Burant, J. M. Millam, S. S. Iyengar, J. Tomasi, V. Barone, B. Mennucci, M. Cossi, G. Scalmani, N. Rega, G. A. Petersson, H. Nakatsuji, M. Hada, M. Ehara, K. Toyota,

R. Fukuda, J. Hasegawa, M. Ishida, T. Nakajima, Y. Honda, O. Kitao, H. Nakai, M. Klene, X. Li, J. E. Knox, H. P. Hratchian, J. B. Cross, C. Adamo, J. Jaramillo, R. Gomperts, R. E. Stratmann, O. Yazyev, A. J. Austin, R. Cammi, C. Pomelli, J. W. Ochterski, P. Y. Ayala, K. Morokuma, G. A. Voth, P. Salvador, J. J. Dannenberg, V. G. Zakrzewski, S. Dapprich, A. D. Daniels, M. C. Strain, O. Farkas, D. K. Malick, A. D. Rabuck, K. Raghavachari, J. B. Foresman, J. V. Ortiz, Q. Cui, A. G. Baboul, S. Clifford, J. Cioslowski, B. B. Stefanov, G. Liu, A. Liashenko, P. Piskorz, I. Komaromi, R. L. Martin, D. J. Fox, T. Keith, M. A. Al–Laham, C. Y. Peng, A. Nanayakkara, M. Challacombe, P. M. W. Gill, B. Johnson, W. Chen, M. W. Wong, C. Gonzalez, J. A. Pople, *Gaussian 03*, Revision C.02, Gaussian, Inc., Wallingford, CT, **2004**.

[30] a) S. C. Lo, C. P. Shipley, R. N. Bera, R. E. Harding, A. R. Cowley, P. L. Burn, I. D. W. Samuel, *Chem. Mater.* **2006**, *18*, 5119–5129; b) C. H. Yang, S. W. Li, Y. Chi, Y. M. Cheng, Y. S. Yeh, P. T. Chou, G. H. Lee, C. H. Wang, C. F. Shu, *Inorg. Chem.* **2005**, *44*, 7770–7780; c) A. B. Tamayo, S. Garon, T. Sajoto, P. I. Djurovich, I. M. Tsyba, R. Bau, M. E. Thompson, *Inorg. Chem.* **2005**, *44*, 8723–8732.

[31] a) P. T. Chou, Y. Chi, *Chem. Eur. J.* **2007**, *13*, 380–395; b) Y. Chi, P. T. Chou, *Chem. Soc. Rev.* **2007**, *36*, 1421–1431; c) E. Y. Li, Y. M. Cheng, C. C. Hsu, P. T. Chou, G. H. Lee, I. H. Lin, Y. Chi, C. S. Liu, *Inorg. Chem.* **2006**, *45*, 8041–8051.

Received: September 19, 2007
Published Online: January 24, 2008

